A SIMPLE LASER BASED PROCESS FOR THE FORMATION OF A LBSF FOR N-TYPE SILICON SOLAR CELLS

Ulrich Jäger, Dominik Suwito, Jan Benick, Stefan Janz, Martin Hermle, Stefan W. Glunz and Ralf Preu
Fraunhofer Institute for Solar Energy Systems (ISE), Heidenhofstrasse 2, 79110 Freiburg i. Brsg., Germany
Phone: +49 (0)761-4588-5536, Fax: +49 (0)761-4588-7812, e-mail: ulrich.jaeger@ise.fraunhofer.de

ABSTRACT: We present a simple laser process for the formation of a local back surface field (LBSF) for *n*-type silicon solar cells. Point contacts are formed by applying a laser process to a doped, passivating layer of amorphous silicon carbide (*PassDop* layer). In a single processing step, point contacts are opened and local doping of the underlying silicon is done. A variation in dopant content and laser fluency enables the control of the doping profile. The effectiveness of the LBSF structure is investigated on lifetime samples. We find that high dopant content of the *PassDop* layer and medium laser fluencies yield best values for the suppression of the recombination at the contact.

Keywords: Laser Processing, n-type, LBSF

1 INTRODUCTION

N-type silicon features several advantages compared to the commonly employed *p*-type silicon: it is less susceptible to common impurities [1, 2] thus leading to higher diffusion lengths in the bulk at a given impurity level. It does not degrade under illumination due to the formation of boron-oxygen complexes. Furthermore, it exhibits a better conductivity at the same doping level as its p-type counterpart, thus yielding more effective high-low junctions in *n*-type silicon.

Commercially available solar cells exceeding a conversion efficiency of 20 % are also using high quality *n*-type material, however employing rather complex cell structures [3, 4]. Glunz *et al*. have outlined the potential for solar cells using *n*-type silicon with simpler cell structures and yielding efficiencies greater than 20 %[5].

On lab scale, Benick *et al*. have demonstrated high efficiencies approaching 24 % fabricating a *P*assivated *E*mitter and *R*ear *L*ocally diffused (PERL) solar cell using *n*-type material [6]. However, the fabrication of the rear local diffusion was done by photolithographic masking and an additional thermal diffusion, making this process unsuitable for industrial fabrication. Thus, an industrial feasible process for a quick and cost effective way to create a LBSF is desirable.

In this work the development of such a process is presented. In the so-called *PassDop* approach, the technique of laser doping is used to create openings in the rear passivation layer and simultaneously create a high doping in the opened silicon bulk.

2 LASER DOPING

2.1 Laser Doping

Laser doping has first been reported on in 1968 as a fast technology to create pn-junctions in silicon [7]. It has been extensively researched in the late 1970's and 1980's [8, 9]. Laser doping is the transient melting of a shallow region of the substrate, as visualized in Figure 1. A prior to laser processing applied precursor is driven into the substrate in the liquid phase.

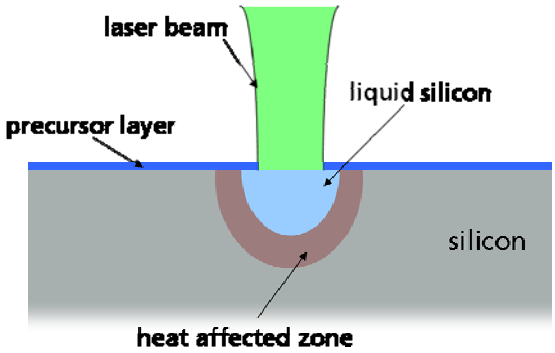

Figure 1: Principle of laser doping: a shallow region of the wafer is molten and a dopant is driven into the silicon during the liquid phase.

This way comparably deep junctions can be fabricated in short time, as the diffusivity in liquid silicon is up to 10 orders of magnitude greater compared to solid state diffusion [10]. The impurity concentration C in the depth z after a diffusion time t is given by

$$C(z,t) = \frac{Q}{\sqrt{\pi Dt}} \exp\left(\frac{-z^2}{4Dt}\right) \quad (1)$$

With Q as the total amount of impurities and the diffusion constant D. Larger pulse energies lead to deeper and longer melting thus reducing the impurity surface concentration for constant Q, as eq. (1) implicates.

For laser fluencies around the melting threshold $\Phi \geq \Phi_m$ a linear increase in melting depth h^l_{max} and thus doping

$$h^l{}_{\max} \cong \frac{l_T}{\sqrt{\pi}} \cdot \frac{\Phi - \Phi_m}{\Phi_m} \quad (2)$$

[11] is expected and has been experimentally observed by other authors [12].

3 LOCAL BACK SURFACE FIELDS (LBSF)

3.1 Increasing the efficiency via the implementation of an LBSF

In the following the importance of a rear side featuring low recombination is briefly outlined using simple calculations employing the 1-diode model. A high

efficient *n*-type PERL solar cell structure is considered. Assuming a high quality *n*-type, 1 Ωcm, $W = 230$ µm thick wafer with a bulk lifetime over 3 ms, Figure 2 illustrates the benefit of reducing the effective recombination velocity on the rear side of the cell S_{eff}. For this cell structure, a high efficiency cell structure is taken into consideration: a high efficiency emitter with an emitter saturation current density of $j_{0e} = 30$ fA/cm² as experimentally shown by Benick *et al.* [6]. For the calculations for the cell efficiency η a fill factor of FF = 80% and a short circuit current density of $j_{SC} = 40$ mA/cm² is assumed. The open circuit voltage is calculated through the 1-diode model

$$V_{OC} = \frac{k_B T}{q} \ln\left(\frac{j_{SC}}{j_{0e} + j_{0b}} + 1\right) \quad (3)$$

with the device temperature T. The base saturation current density j_{0b} is obtained from

$$j_{0b} = \frac{qD_h n_i^2}{N_D L} \times \frac{S_{eff}\cosh\left(W/L\right) + D_h/L \sinh\left(W/L\right)}{D_h/L \cosh\left(W/L\right) + S_{eff}\sinh\left(W/L\right)} \quad (4)$$

[13] with q the elementary charge, D_h the minority carrier diffusivity, N_D the equilibrium hole density, L the minority carrier diffusion length and n_i the intrinsic charge carrier density.

If low values for S_{eff} are considered, a strong decrease in the recombination loss is visible (i.e. increase in V_{OC}), thus yielding a considerable gain in cell efficiency η. For the high efficiency cell scheme, a reduction of S_{eff} below 20 cm/s yields efficiencies greater than 22 % and an open circuit voltage V_{OC} beyond 685 mV. Therefore, an outstanding passivation with point contacts contributing only little to the overall base saturation current is highly desirable.

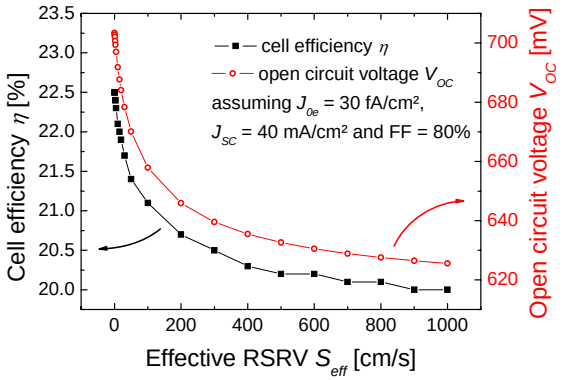

Figure 2: Dependence of the open circuit voltage V_{OC} and cell efficiency η on the effective rear side recombination velocity for a high efficiency n-type PERL solar cell

3.2 The *PassDop* approach

To reduce the recombination at the back side of the device a high doping underneath the metal contacts is favorable using a field effect passivation of the contacts induced by the high-low junction. For the formation of local point contacts with a shallow BSF the technique of Laser Fired Contacts (LFC) [14] was developed. However, it is not suited for *n*-type silicon, as aluminum cannot form a high-low junction in *n*-type silicon. Therefore, a new approach using the technique of laser doping has been developed and is schematically shown in Figure 3. It is combining doping from and opening of a phosphorous doped passivating layer and is thus referred to as "*PassDop*". The *PassDop* layer is a doped amorphous silicon carbide film serving both as a passivation and doping precursor layer.

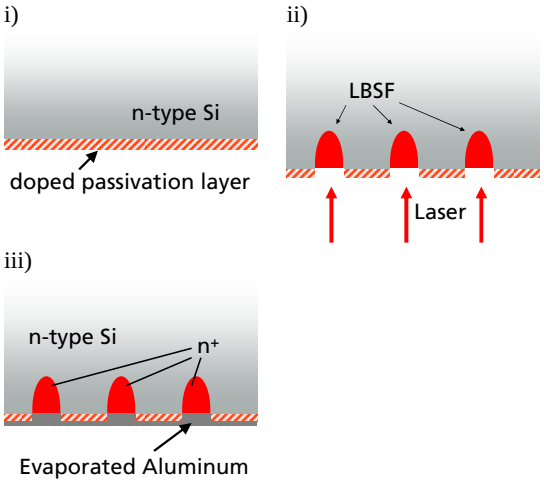

Figure 3: Process scheme of the *PassDop* approach: after cleaning, (i) a doped passivation layer is deposited onto the rear side of the wafer, (ii) a laser opens point contacts in the passivation layer and simultaneously dopes the substrate subsequently (iii) aluminum is evaporated on top finishing the rear side of the device [15].

4 SAMPLE PREPARATION

4.1 *p*- and *n*-type wafers

Two kinds of samples were prepared (figure 4): (i) to investigate the doping results, the phosphorous amorphous silicon carbide layer was deposited on a single side of a 250 µm thick, 1 Ωcm p-type FZ silicon to enable an emitter formation after laser processing. These samples are discussed in sections 5.1 and 5.2. (ii) To quantify the formation and effectiveness of the high-low junction point contacts, the a-SiC layers were deposited on both sides of FZ, 1 Ωcm, 230 µm thick n-type wafers yielding symmetrical samples, allowing a measurement of the effective lifetime by means of quasi-steady state photo conductance technique (QSSPC) [16].

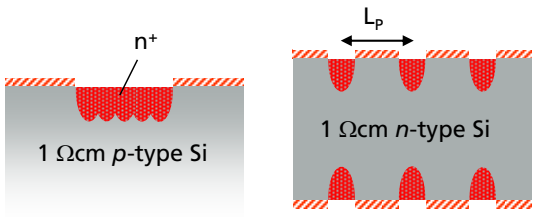

Figure 4: Left: Samples prepared for the investigation of the doping (i) and Right: samples prepared for testing the local point contacts (ii)

4.2 Layer deposition

For the PECVD deposition of the amorphous silicon carbide films in this work, we used a Roth&Rau AK400M reactor featuring a high-frequency (13.65 MHz) as well as a microwave (2.4 GHz) generator as

plasma sources. As precursor gases silane (SiH_4) and methane (CH_4) were used. Highly diluted phosphine (PH_3) was used as a dopant source for incorporating phosphorous into the layer. All samples were wet-chemically cleaned prior to the PECVD process with a short dip in HF. The layer thickness was 30-40 nm. Three different gas fluxes of PH_3 were chosen, denominated in the following as low, medium and high [15].

4.3 Laser Processing

Laser processing was done with a disc laser at a wavelength of 1030 nm at a repetition rate of 15 kHz using a galvanometer scanner for positioning the laser beam on the wafer. The pulse energy was controlled by a variable optical attenuator, insuring the stability of all beam parameters other than the fluence. For the samples (i) a 20x20 mm² area was homogenously doped to allow an analysis of the sheet resistance by a 4-point-probe and the acquisition of the doping profiles. The pulse overlap was kept small to ensure similar conditions as they occur in doping point contacts. For the investigations of the point contacts (samples (ii)), points were set apart with a constant spacing of L_P = 1 mm. The effective lifetime τ_{eff} was measured before and after laser processing, allowing the extraction of S_{eff} via [17]

$$\frac{1}{\tau_{eff}} = \frac{1}{\tau_{bulk}} + \frac{2S_{eff}}{W} \qquad (5)$$

with the sample thickness W and τ_{bulk} the lifetime of the bulk material, determined from the intrinsic lifetime limit using the model of Kerr [18].

5 RESULTS

5.1 Sheet resistance

Figure 4 shows the measured sheet resistances for the samples of type (i). Each data point represents the mean value of 9 measurements; the error bar is their standard deviation, thus also providing some information about the homogeneity of the process.

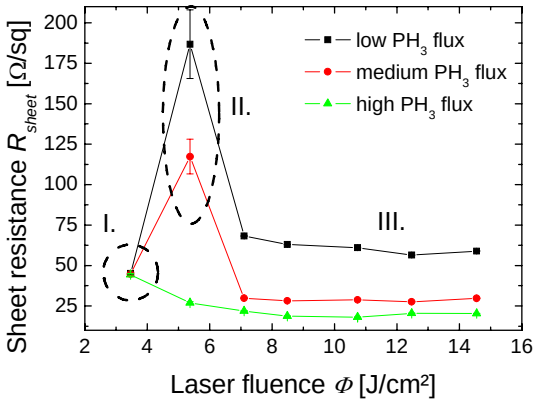

Figure 4: Evolution of the sheet resistance with increasing laser fluence Φ. After crossing the melting threshold, the sheet resistance changes only little for a given precursor layer. The three different PH_3 gas fluxes are shown. The three regions are explained in the text.

Region I. marks the region below the melting threshold. No laser doping has taken place. The points around 5.5 J/cm² (region II.) mark the beginning of the surface melting. High sheet resistances and very high standard deviations point out that only little doping has taken place and the process is not yet stable, as it is right at the melting threshold. In region III. a constant sheet resistance is reached for each dopant gas flux. The more dopant is available; the lower is the sheet resistance. In this regime all the available dopant is driven into the substrate and only minor changes in sheet resistance occur due to different doping profiles.

5.2 Doping profiles

In Figure 5 the resulting doping profiles acquired by means of spreading resistance profiling (SRP) for the medium gas flux of PH_3 are shown. The doping depth increases with increasing laser fluence. The step like behavior of the curves is due to an averaging over 10 points of measurement of the carrier density N.

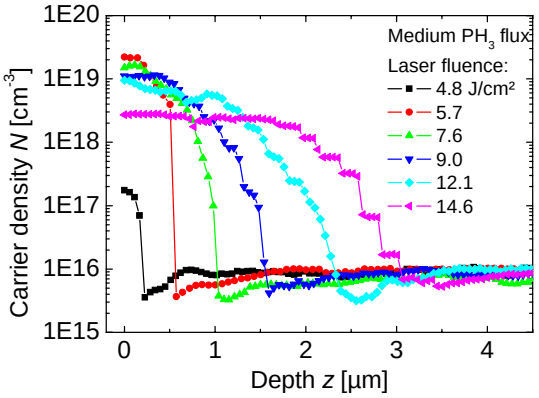

Figure 5: Resulting doping profiles after laser irradiation. The profiles displayed are for the medium flux of PH_3 [15].

Figure 6 depicts the doping depth at 1e16 cm^{-3} as well as the integrated amount of phosphorous. As expected from eq. (2) the doping depth increases linearly in this regime of fluencies. The integrated amount of phosphorous is constant even at higher fluencies, indicating that only little or no ablation of the *PassDop* layer takes place during the laser process at medium fluencies.

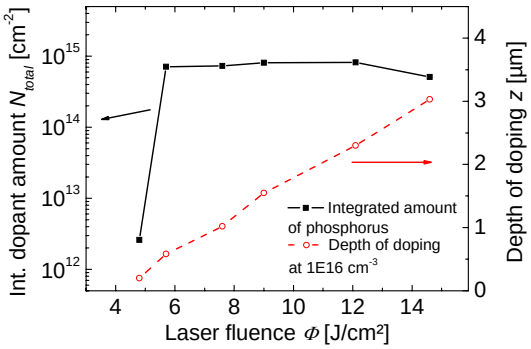

Figure 6: Integrated amount of phosphorous after laser doping and depth of doping at 1e16 cm^{-3} [15].

5.3 Investigation of S_{cont}

Fischer has proposed a model to quantify the effective recombination velocity at the rear surface of a point contacted solar cell [19]. The effective rear surface

recombination velocity S_{eff} is given by

$$S_{eff} = \frac{D_h}{W}\left[\frac{L_p}{2W\sqrt{\pi f}}\arctan\left(\frac{2W}{L_p}\sqrt{\frac{\pi}{f}}\right) - \exp\left(-\frac{W}{L_p}\right) + \frac{D_h}{fWS_{cont}}\right]^{-1} + \frac{S_{pass}}{1-f} \quad (6)$$

with W the cell thickness, L_p the pitch of the point contacts, $f = \pi r^2/L_p^2$ the metallization fraction, determined by the fraction of the area of the point contact (with radius r) over the square of the pitch, D_h the diffusivity of the minorities (holes), S_{cont} the recombination velocity at the contact and S_{pass} the recombination velocity of the passivated areas. Note that S_{cont} is considered as the recombination velocity at the opening. Although no metal is applied in this investigation, bare silicon features similar surface recombination as for a metal coated surface.

By measuring the effective lifetime of the samples (ii) before and after laser processing at an excess carrier density of Δn = 5e14 cm^{-3} S_{pass} and S_{eff} can be determined via eq. (5). For each fluence, the contact radius r and thus the metallization fraction f is measured. These values are put into eq. (6) and it is solved for S_{cont}, giving a measure for the recombination at the point contacts. This is depicted in Figure 7.

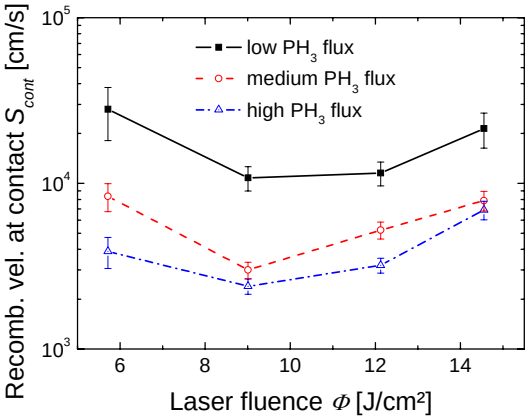

Figure 7: Recombination velocity at the contact S_{cont} as a dependence of the laser fluence Φ and with the gas flux as a parameter [15].

An optimum value for S_{cont} can be ascertained for the high PH_3 flux and medium laser fluence. A minimum value of 2400 (+/-250) cm/s is reached for 9 J/cm² and high gas flux. The error indicated accounts for the uncertainty of determining the contact radius r of the point contacts with an accuracy of +/- 1 µm. It is observed that the best values for S_{cont} are obtained for the high gas flux over the entire range of laser fluencies.

The application of this process to a high efficient *n*-type PERL cell structure leads to open circuit voltages beyond 700 mV and efficiencies over 22 % [20].

6 SUMMARY

A laser based process for the formation of a local back surface field for *n*-type silicon solar cells has been developed. In the presented approach a layer of phosphorous doped amorphous silicon carbide serves both as a passivation and dopant source (*PassDop*). The contact opening and doping can be done with a suitable laser process, i.e. in a single processing step. By adjusting the laser parameters and the content of the doping in the *PassDop* layer, the resultant doping profile can be adjusted. Calculation of the RSRV at the local contacts yields values down to 2400 cm/s.

The PassDop sequence is a very simple process for the passivation of the rear of the cell and for the formation of a local back surface field for n-type silicon solar cells with a high efficient PERL cell structure. As the formation of the LBSF and the contact opening is done in one single step, this process is of considerable interest for a possible future high volume production for *n*-type silicon solar cells. Its application to a high efficient PERL solar cell structure has led to open circuit voltages exceeding 700 mV and efficiencies well above 22% [20].

ACKNOWLEDGEMENTS

The authors thank P. Saint-Cast for the fruitful discussion of the findings and A. Kremer for the support in the measurements. The work was supported by the German Federal Ministry for the Environment, Nature Conservation and Nuclear Safety under contract number 0329849A “Th-ETA”.

REFERENCES

1. Macdonald, D. and Geerligs, L.J., *Recombination activity of interstitial iron and other transition metal point defects in p- and n-type crystalline silicon.* Applied Physics Letters, 2004. **85**(18): p. 4061-3.
2. Glunz, S.W., Rein, S., Lee, J.Y., and Warta, W., *Minority carrier lifetime degradation in boron-doped Czochralski silicon.* Journal of Applied Physics, 2001. **90**(5): p. 2397-404.
3. Tsunomura, Y., Yoshimine, Y., Taguchi, M., Baba, T., Kinoshita, T., Kanno, H., Sakata, H., Maruyama, E., and Tanaka, M., *Twenty-two percent efficiency HIT solar cell.* Solar Energy Materials & Solar Cells, 2009. **93**(6-7): p. 670-3.
4. P.J. Cousins, D.D.S., H.-C. Luan, J. Manning, T. D. Dennis, A. Waldhauer, K. E. Wilson, G. Harley, W. P. Mulligan. *Generation 3: Improved Performance at lower Cost*. in *35th IEEE PVSC*. 2010. Honolulu, Hawaii, USA.
5. Glunz, S.W., Benick, J., Biro, D., Bivour, M., Hermle, M., Pysch, D., Rauer, M., Reichel, C., Richter, A., Rüdiger, M., Schmiga, C., Suwito, D., Wolf, A., and Preu, R. *n-type silicon - enabling efficiencies > 20% in industrial production*. in *Proceedings of the 35th IEEE Photovoltaic Specialists Conference*. 2010. Honolulu, Hawaii, USA.
6. Benick, J., Hoex, B., Dingemans, G., Richter, A., Hermle, M., and Glunz , S.W. *High-efficiency n-type silicon solar cells with front side boron emitter*. in *Proceedings of the 24th European*

Photovoltaic Solar Energy Conference. 2009. Hamburg, Germany.
7. Fairfield, J.M. and Schwuttke, G.H., *Silicon diodes made by laser irradiation.* Solid State Electronics, 1968. **11**: p. 1175-6.
8. Wood, R.F., Kirkpatrick, J.R., and Giles, G.E., *Macroscopic theory of pulsed-laser annealing. II. Dopant diffusion and segregation.* Physical Review B, 1981. **23**(10): p. 5555-69.
9. Fogarassy, E., Stuck, R., Toulemonde, M., Salles, D., and Siffert, P., *A model for laser induced diffusion.* Journal of Applied Physics, 1983. **54**(9): p. 5059-63.
10. Kodera, H., *Diffusion coefficients of impurities in silicon melt.* Japanese Journal of Applied Physics, 1963. **2**(4): p. 212-9.
11. Bäuerle, D., *Laser processing and chemistry*. 3rd ed. 2000, Linz: Springer. 788.
12. Bruines, J.J.P., van Hal, R.P.M., Boots, H.M.J., Sinke, W., and Saris, F.W., *Direct observation of resolidification from the surface upon pulsed-laser melting of amorphous silicon.* Applied Physics Letters, 1986. **48**(19): p. 1252-4.
13. Goetzberger, A., Voß, B., and Knobloch, J., *Sonnenenergie: Photovoltaik, Physik und Technologie der Solarzelle*. 2nd ed. 1997, Stuttgart: Teubner. 261.
14. Schneiderlöchner, E., Preu, R., Lüdemann, R., and Glunz, S.W., *Laser-fired rear contacts for crystalline silicon solar cells.* Progress in Photovoltaics: Research and Applications, 2002. **10**: p. 29-34.
15. Jäger, U., Suwito, D., Benick, J., Janz, S., and Preu, R., *A Novel Laser Based Process for the Formation of a LBSF for n-type Silicon Solar Cells.* submitted to Thin Solid Films, 2010.
16. Sinton, R.A. and Cuevas, A., *Contactless determination of current-voltage characteristics and minority-carrier lifetimes in semiconductors from quasi-steady-state photoconductance data.* Applied Physics Letters, 1996. **69**(17): p. 2510-2.
17. Cuevas, A. and Macdonald, D., *Measuring and interpreting the lifetime of silicon wafers.* Solar Energy, 2004. **76**(1-3): p. 255-62.
18. Kerr, M.J. and Cuevas, A., *General parameterization of Auger recombination in crystalline silicon.* Journal of Applied Physics, 2002. **91**(4): p. 2473-80.
19. Fischer, B., *Loss analysis of crystalline silicon solar cells using photoconductance and quantum efficiency measurements*, in *Fachbereich Physik*. 2003, Universität Konstanz: Konstanz. p. 198.
20. Suwito, D., Jäger, U., Benick, J., Janz, S., Hermle, M., and Glunz, S.W., *Industrially Feasible Rear Passivation and Contacting Scheme for High-Efficiency n-Type Solar Cells Yielding a Voc of 700 mV.* IEEE Transactions on Electron Devices, 2010. **57**(8): p. 2032-2036.